arXiv:astro-ph/0106431v1 23 Jun 2001

On the Metallicity of Star-forming Dwarf Galaxies

Francois Legrand,[1] Guillermo Tenorio-Tagle,[2] Sergey Silich,[2,3] Daniel Kunth,[1] and Miguel Cerviño [4]

ABSTRACT

We construct three extreme different scenarios of the star formation histories applicable to a sample of dwarf galaxies, based either on their present metallicity or their luminosity. The three possible scenarios imply different mechanical energy input rates and these we compare with the theoretical lower limits established for the ejection of processed matter out of dwarf galaxies. The comparison strongly points at the existence of extended gaseous haloes in these galaxies, acting as the barrier that allows galaxies to retain their metals and enhance their abundance. At the same time our findings strongly point at a continuous star-forming process, rather than to coeval bursts, as the main contributors to the overall metallicity in our galaxy sample.

Subject headings: ISM: bubbles, ISM: abundances, general - starburst galaxies

1. Introduction

Given the extreme violence of stellar ejection processes, either through supernova explosions or strong stellar winds, the presence of strong reverse shocks assures that upon thermalization the ejected matter would reach temperatures ($T \sim 10^6 - 10^8$ K) that would strongly inhibit recombination, and thus the detection of the newly processed material at optical and radio frequencies. Furthermore, it is now well understood that this hot high pressure gas fills the interior of superbubbles and drives the outer shock that sweeps and accelerates the surrounding ISM into an expanding large-scale supershell. The continuous energy input rate from coeval starbursts or continuous star forming phases, due to last until the last 8 $M_\odot$ star explodes as supernova, reassures that the high temperature of the ejected matter is maintained above the recombination limit ($T \sim 10^6$ K) allowing superbubbles to reach dimensions in excess of 1 kpc. During this time the highly metal enriched superbubble gas does not diffuse either in the expanding shell nor in its immediate surroundings. It has been convincingly argued in recent years that the metallicity detected in star-forming galaxies results from their previous history of star formation and has nothing to do with the metals presently ejected by their powerful starbursts (see Tenorio-Tagle 1996). One in fact would have to wait until the end of the supernova phase (≥ 40 Myr) for the full ejection of all heavy elements synthesized by the massive stars. At this stage up to almost 40% of the starburst mass would have been returned to the ISM and heavy elements, such as oxygen, would have reached their expected yield value.

Note that the newly processed heavy elements are generated within a region of about 100 pc (the typical size of starburst) while upon cooling of the superbubble interior and their fall back towards the galaxy, the heavy elements are disseminated over a region of several kpc in size. After such a large-scale dispersal, diffusion leads to a thorough mixing of the heavy elements within the host galaxy ISM, enhancing its metallicity.

Indeed the final step towards mixing within the ISM is promoted by diffusion since diffusion is largely enhanced in high temperature gases.

---

[1] Institut d'Astrophysique de Paris; 98bis Boulevard Arago, 75014 Paris, France

[2] Instituto Nacional de Astrofísica Optica y Electrónica, AP 51, 72000 Puebla, Mexico

[3] Main Astronomical Observatory National Academy of Sciences of Ukraine, 03680 Kiyv-127, Golosiiv, Ukraine

[4] Observatoire Midi Pyrènées; 14, avenue Edouard Belin, 31400 Toulouse, France

Therefore, if a new major centre of star formation develops and causes the formation of an HII region, the heavy elements will rapidly mix to produce a uniform abundance. In the absence of star formation however, the heavy element droplets will also diffuse but over larger time-scales (see Tenorio-Tagle 1996). All together the process of mixing takes several 4 - 6 $\times$ 10^8 yr to promote an enhanced and almost uniform abundance in a region of up to several kpc in radius around the original starburst.

On the other hand, the observational evidence of powerful starbursts in dwarf galaxies has led to the idea that, due to their rather shallow gravitational potential, supernova products and even the whole of the interstellar medium, may be easily ejected from the host dwarf systems, causing the contamination of the intra-cluster medium (Dekel & Silk 1986; De Young & Heckman 1994). However, the indisputable presence of metals (in whatever abundance) in galaxies implies that the supernova products cannot be completely lost in all cases.

This issue has been recently addressed by Silich & Tenorio-Tagle (2001; hereafter referred to as Paper I) and D'Ercole & Brighenti (1999) who show that within a dark matter (DM) and a low-density extended gaseous halo, a galactic wind does not easily develop, making the removal of the galaxy's ISM very inefficient. Here we compare the theoretical estimates with some well known starbursts in blue compact dwarf (BCD) galaxies. In particular we derive three different possible star formation history scenarios that assume either a very young coeval starburst or an extended phase of star formation of 40 Myr or 14 Gyr, to account for the inferred star formation rate (in the first two cases) and the observed metallicity (in the third one) from our sample galaxies. For these galaxies we know: their HI mass, metallicity and Hα or Hβ luminosities, and these allow us to infer the energy input rate expected in each of our galaxies, for each of the three likely histories of star formation (see Section 2). Section 3 is devoted to a comparison of the energy input rates derived for our galaxies with the recent estimates of the rates required to expel either metals or the ISM from galaxies containing a total ISM mass in the range of 10^6 to 10^{10} $M_\odot$ (see Paper I). Section 4 gives a discussion of our results.

2. The Star forming history of BCD galaxies

Our sample of dwarf galaxies (see Table I) was selected from Papaderos et al (1996), Mas-Hesse & Kunth (1999), Marlowe, Meurer & Heckman (1999), Lequeux et al. (1979). We took care to exclude galaxies which could be tidal dwarfs, because in such a case their metallicity would not be the result of the evolution of the present day system. The sample also includes a few dIrr galaxies from Skillman, Kennicutt & Hodge (1989). In Table 1 the first column provides the galaxy identification and columns 2 and 4 give the HI mass and metallicity as reported in the references given in columns 3 and 5, respectively. The fact that many galaxies, such as IZw 18 (Vilchez & Iglesias-Paramo, 1998; Legrand *et al.* 2000; see also van Zee *et al.* 1998), IIZw 40, NGC 4214 (Kobulnicky & Skillman 1996), NGC 1569 (Devost *et al.* , 1997), and others, present a uniform metal abundance within their HII region gas, irrespectively of the chosen slit location, and the arguments given in section I regarding the unlikely possibility that the metals come from the present generation of stars, have led us to assume that galaxies have been evenly polluted throughout their histories, up the levels now displayed in their HII region gas.

We examine three different scenarios of the star formation using the observed properties of our sample of dwarf galaxies. For our first two models, the observed H_α luminosities (column 6 of Table 1) were used to estimate the gas mass converted in stars. We derive the UV photon output from the exciting cluster using Leitherer & Heckmann (1995) (hereafter referred to as LH95) relation $L(H\alpha)$ erg s^{-1} $= 1.36{\times}10^{-12}N(H^0)$ s^{-1}, and then convert it into the SFR. References to the observed Hα luminosity are given in column 7 of Table 1. These correspond to the total luminosity obtained from digital photometry on CDD images using an Hα filter. Whenever the Hα luminosity of a galaxy was not available, we used Hβ instead and using the relation: Hα/Hβ = 2.857, as in LH95. Galaxies for which the Hα luminosity has been inferred from their Hβ luminosity are marked with an asterisk in the column 7 of Table 1. In these cases, it can be assumed that the observed Hβ flux also corresponds to the total flux, either because the slit apperture has been chosen large enough for a realistic comparison with *IUE* data (Mas-Hesse & Kunth, 1999, Storchi-Bergmann, Kinney, Challis, 1995), or photometrically derived from CDD images (Vilchez, 1995 Gallagher, Hunter & Bushouse, 1989).

We have first assumed that all stars have resulted from a coeval burst. Under these conditions, it is well known that the mechanical input rate through winds and supernovae leads to an almost immediate constant value to be maintained throughout the supernova phase (4 $\times 10^7$ yr). On the other hand the ionizing flux is to remain constant at its maximum value only for the first 3.5 Myr, and then decreases as t^{-5} (see Beltrametti *et al.* 1981). The implication of this rapid decay is that after 10^7 yr the UV photon output is two orders of magnitude smaller than its original value, and thus the HII region phase is much shorter than the supernova phase. Here we assume that our clusters are indeed coeval and young ($\leq$ 3.5 Myr). The Hα luminosity is also in this case a direct indicator of the number of ionizing photons. However, to infer the mass of the starbursts, the number of ionizing photons should be linearly scaled using Figure 37 of LH95, which gives a value of $N(H^0) \sim 10^{53}$ photons s^{-1} for every 10^6 M$_\odot$ of stars formed. The corresponding mechanical energy input rate can thus be evaluated using the calibration given by these authors for an instantaneous burst of 10^6 M$_\odot$ (LH95, their Figure 55). The values found for the mass in stars and mechanical energy injection rate are given in column 2 and 3 of Table 2, for each entry.

In this model, our mass estimates will be wrong by a factor of ten if the age of our starbursts would be 6.5 Myr, and by a factor of 100 if they all are 10 Myr old. The presence of strong Wolf-Rayet features in the spectra of many of the sources in the sample, as in IZw 18, (see Kunth & Ostlin 2000, and references therein) certifies however their young age ($\sim$ 3.5 Myr).

In our second model the present star formation rate was assumed to be continuous for the last tens of Myr. In this case, the ionizing photon output reaches a maximum constant value after 3 - 4 Myr while the mechanical luminosity of the starburst rises to reach its asymptotic maximum value only after 40 Myr (LH95). We thus use their continuous star formation model to derive the SFR from the number of ionizing photons ($N(H^0)$) as well as the corresponding energy injection rate, assuming a continuous and constant SFR over the last 40 Myr (LH95, Figures 38 and 56). The resultant SFR and the corresponding mechanical energy input rate for each of our galaxies are given in columns 4 and 5 of Table 2. Note that despite the fact that there is no information on the time since star formation began in our galaxies, our assumption that $t \geq 40$ Myr, leads to an upper limit for the mechanical energy input rate as implied from the derived SFR.

In models 1 and 2, we have assumed that all the ionizing photons produced by the stellar clusters are completely used up in the ionization of the HII region gas. Note however that if a fraction of these, say 50%, manage to freely escape the nebulae, or are absorbed by dust, our final estimates are only off by a factor of two.

For our third model we have evaluated the amount of stars required to produce the observed oxygen abundance in each galaxy of our sample. Because this approach is based on the entire galaxy evolution, we used here a closed box model and the instantaneous recycling approximation despite of the time delay between the metal ejection and their complete mixing with the galaxy ISM. In the low metallicity limit (or for large remaining gas fraction $\mu = \frac{M_{gas}}{M_{gas}+M_{stars}}$) the ISM gas metallicity Z is given by:

$$Z = -y \ln(\mu) \qquad (1)$$

where y is the net yield (Maeder, 1992). This approximation is valid for all the objects in our sample. For oxygen this relation becomes:

$$\frac{O}{H + He + metals} = -y_O \ln\left(\frac{M_{gas}}{M_{gas} + M_{stars}}\right) \qquad (2)$$

where y_O is the oxygen yield. As we only have a measurement of the hydrogen content, we have assumed a constant He/H ratio: $M_{gas} = M_{HI+He} = 1.34\, M_{HI}$ (Kunth & Sargent 1986).

Thus, reverting equation 2 we can derive the mass of stars required to produce the observed oxygen abundance in our objects, as a function of their HI mass and the oxygen yields.

It is important to notice that the derived mass in stars is a lower limit. Indeed, under the assumption of a closed box model, all of the metals produced remain within a galaxy and contribute to globaly enhance its metallicity. If some of the metals could escape into the intergalactic space, the amount of stars needed to produce the actual measured metallicities will have to be larger. Of course, this mass also depends on the yields used, and the normalization of the yields depends on the adopted initial mass function. Here we used the oxygen yield $Y_O = 0.0026$ computed from Maeder (1992) models for an initial mass function with a power law index -2.35 between 0.1 $M_\odot$ and 120 $M_\odot$. The evaluated stellar mass in the range 1-120 $M_\odot$ needed to produce the observed global metallicity of our galaxies is given in column 6 of Table 2.

In the last scenario we have assumed that star formation has taken place all over the volume of the host galaxies. We have then divided the derived stellar masses by 14 Gyrs to compute the continuous star formation rate required to produce the observed metallicity over a Hubble time. This star formation rate is given in the column 7 of Table 2. Note that this scenario leads to a lower limit for the mechanical energy injection rate. Indeed, if the same amount of stars were formed during burst events, the expected mechanical energy input rate should become momentarily larger.

The corresponding mechanical energy injection rate (column 8 of Table 2) was computed using the normalization $log(L_{mech})$ erg s^{-1} = 41.8. This is a mean value predicted by a continuous starburst model, for different star metallicities, after the equilibrium regime is reached (see Figure 56 of LH95) under the assumption of a Salpeter initial mass function between 1 and 100 $M_\odot$ and star formation rate of 1 $M_\odot$ yr^{-1}. Therefore we have used this value for our sample regardless of the galaxy metallicity.

Note that if a continuous star formation process, spread over the whole galaxy volume and over a Hubble time, is required to produce the observed global abundances detected in our galaxies, then the implied SFRs and total mechanical luminosities are comparable to the values derived for either our model 1 or 2. This is remarquable since for models 1 and 2, the SFR, the mass in stars, and the mechanical luminosities were inferred independently from the present–day galaxy luminosity. Although metals presently being produced are hidden from view (at least in the optical regime) because the recombination process is inhibited at high temperatures when crossing the reverse shocks (see section I), we can derive, for each galaxy, the number of "typical" starburst events similar to the present ones, required to account for the observed metallicities. If one divides the stellar mass implied by chemical evolution (column 6 in Table 2) over the starburst mass derived in scenarios 1 and 2, one would find the number of events needed to explain the metal content, evenly spread over the galactic volumes. Column 9 of Table 2 provides the number of extended (40Myr) or coeval bursts, required to account for the metallicity of the galaxies in our sample. Note that the derived numbers of bursts are also a lower limit estimate as the closed box model provides a lower limit on the stellar mass. Nethertheless, the large number of bursts required in most of the cases, both in models 1 and 2, simply reflects the fact that it is the whole galactic volume what aught to be contaminated. These large numbers seem unrealistic and thus one is lead to conclude that the main agent causing the global metallicity present in galaxies is a uniform, constant and long-lasting SFR, spread (as in model 3) over the galaxy volume. Starbursts may take place throughout the history of the galaxy, with a star–forming activity similar to what is found in the whole galactic volume, however, their contribution to the total metallicity would not be the most significant.

Finally, we compared the values of the derived mechanical energy injection rate in the three considered cases, with the predictions of the hydrodynamical models of McLow & Ferrara (1999) and Silich & Tenorio-Tagle (2001). The results are shown in Figure 1.

3. Comparison with the theoretical estimates

3.0.1. The energy requirements

Figure 1 shows our energy estimates resultant from the numerical integration of the hydrodynamic equations for a coeval starburst with a constant energy input rate during the first 4 $\times 10^7$ yr of the evolution, acting on an ISM density distribution with a total mass in the range of 10^6 to 10^{10} $M_\odot$. Two extreme density distributions were assumed: either rotating flattened disks (lower two lines) or spherical galaxies without rotation (upper two lines; see Paper I). Clearly disk-like models require less energy to eject their metals into the intergalactic medium. This is because the amount of interstellar gas that has to be blown out of a disk-like galaxy to open a channel for metal ejection into the intergalactic medium is much smaller than in the spherically symmetric limit, where all of the metal-enriched ISM has to be accelerated to reach the galaxy boundary.

In Figure 1, values below each line imply total retention, while the region above each line indicates the expulsion of the hot superbubble interior gas (with the new metals) out of disk-like distributions, and of the new metals and the whole of the ISM in the spherical cases. Each line that separates the two regions marks the minimum energy input rate needed from a coeval starburst to reach the outer boundary of a given galaxy with a supersonic speed, regardless of the time that the remnant may require to do so (see Paper I).

The energy input rates derived for our sample of galaxies (see Table 2) in each of the three star formation scenarios here considered have been incorporated in panels 1a - 1c. Note that the energy input rate derived in model 3 from the continuous star formation activity able to account for the metallicity of the host galaxies, although originally assumed to take place all over the galaxy volume is here compared with the theory estimates derived for spatially concentrated starbursts.

4. Discussion

Based on sound observed facts such as the HI mass, metallicity and either the Hα or Hβ luminosity of star-forming dwarf galaxies we have constructed three different likely scenarios for their star formation histories. The various extreme possibilities result from considering either young coeval starbursts or extended phases of star formation lasting 40 Myr and 14 Gyr respectively.

For the coeval starburst scenario, as well as for the second extended and constant star formation rate model, the star formation rate and the total mass of the starburst have been inferred from the observed Hα and Hβ luminosity of each of the galaxies. The third scenario assumes a constant star formation rate over a Hubble time (14 Gyr), as low as it is required to account for the observed metallicity in each of these galaxies. Based on the synthetic properties of coeval and extended starbursts we have inferred the energy input rate to be expected in each of the cases and these have been compared with the recent theoretical estimates of the minimum energy input rate required to vent the processed matter into the intergalactic medium (see Paper I).

In all three star formation history scenarios, all galaxies in our sample lie above the lower limit first derived by Mac Low & Ferrara (1999), and then confirmed in Paper I, for the ejection of metals out of flattened disk-like ISM density distributions when energized by relatively low mass starbursts. Under these assumptions, the observed metallicity in these systems cannot be accounted for. Our results however, place the bulk of our sample, in all three considered star formation history scenarios, below the minimum energy input rate range of values derived for galaxies that present an extended low density gaseous halo. And thus, as shown in Paper I, it seems to be the mass of the extended low density halo, the one that acts as the barrier against metal ejection into the IGM.

Note that in the 14 Gyr extended star formation case, all galaxies lie below the lower limit imposed by the presence of an extended low density halo (see Figure 1c). A few objects namely: NGC 1569, IZw 18, Haro 2, and Mrk 49 surpase this lower limit in the case of a 40 Myr extended star formation history (see Figure 1b), as it is also the case of NGC 1569 in the coeval starburst scenario (see Figure 1a). These facts imply that the limit derived by Silich & Tenorio-Tagle (2001) is indeed a lower limit as it does not consider all possible phases of the ISM, nor magnetic fields and it has (as other models in the literature) assumed a constant energy input rate. All of these are issues that if thoroughly considered could substantially raise the energy input rate required for mass ejection out of dwarf galaxies hence the metals are indeed trapped in all cases. A second possibility is that if the metallicity in these galaxies results from several extended star formation phases, or from several coeval bursts (see column 9 of Table 2), the metals produced by the present phase of star formation will only in a few of the cases be able to escape into the IGM.

However, given the large number of star formation events that have been derived for many of our galaxies in both models 1 and 2, it is obvious that the main contribution to the global metallicity measured in star-forming dwarf galaxies is due to a long-lasting and continuous star forming process, spread over the whole galaxy volume. A few coeval and massive bursts, similar to the ones presently energizing the galaxies, may occur throughout history. Taking 100 Myr time interval between the sequential starbursts, one can find, that in most of the galaxies from oursample, instantaneous starburst may account for 1/10 or even much less of the detected metal abundances.

The main implication of our results is that one has to invoke the existence of extended gaseous haloes in order to account for the metals present in galaxies. Predicted haloes, despite acting as a barrier to the loss of the new metals, have rather low densities ($< n_{halo} > \sim 10^{-3}$ cm^{-3}) and thus have a long recombination time ($t_{rec} = 1/(\alpha n_{halo})$; where α is the recombination coefficient) that can easily exceed the lifetime of the HII region ($t_{HII} = 10^7$ yr) developed by the starburst. In such a case, the haloes may remain undetected at radio and optical frequencies (see Tenorio-Tagle et al. 1999), until large volumes are collected into the expanding supershells. Note that the continuous Ω shape that supershells present in a number of galaxies, while remaining attached to their central starburst, as well as their small expansion velocity (comparable or smaller than the escape velocity of their host galaxy) imply that the mechanical energy of the star cluster is plowing into a continuous as yet undetected medium. Furthermore, in the presence of a halo, it is the mass of the halo what sets the limiting energy input rate required for mass ejection into the IGM, and not the mass of the disk-like component. This argument applies to all galaxies whether spirals, amorphous, irregulars or dwarfs.

The authors acknowledge Miguel Mas Hesse and Michel Fioc for fruitful comments and suggestions. We specially acknowledge the useful remarks of the anonymous referee that helped to improve the clarity of the paper. GTT thanks CONACYT for the grant 211290-5-28501E which allowed for the completion of this study, and MC is supported by an ESA postdoctoral fellowship.

REFERENCES

Becker R., Mebold, U., Reif, K. & van Woerden, H., 1988, A&A 203, 21

Beltrametti M., Tenorio-Tagle G. & Yorke, H. W., 1982, A&A, 112, 1

Contini, T., 1996a, in Wolf-Rayet stars in the framework of stellar evolution. Liege: Universite de Liege, Institut d'Astrophysique. Edited by J.M. Vreux, A. Detal, D. Fraipont-Caro, E. Gosset, and G. Rauw, p.619

Contini, T., 1996b, Ph.D. Thesis, Universite Paul Sabatier, Toulouse, France

D'Ercole, A. & Brighenti, F., 1999 MNRAS 309, 941

Dekel, A. & Silk, J., 1986, ApJ, 303, 39

De Young, D. & Heckman, T., 1994, ApJ, 431, 598

Devost, D. Roy, J-R. & Drissen, L., 1997 ApJ 482, 765

Gallagher, J. S., Hunter, D.A. & Bushouse, H., 1989, AJ 97, 700

Huchtmeier, W. K., Karachentsev, I. D., Karachentseva, V. E. & Ehle, M., 2000, A&AS 141, 469

Hunter, D. A., Hawley, W. N. & Gallagher, J. S. III, 1993, AJ 106, 1797

Karachentsev, I. D., Makarov, D. I. & Huchtmeier, W. K., 1999, A&AS 139, 97

Kobulnicky, H. A. & Skillman, E., 1996 ApJ 471, 211

Kunth, D. & Ostlin, G., 2000 A&AR 10, 1

Kunth, D. & Sargent, W. L. W., 1986, ApJ 300, 496

Legrand, F., Kunth, D., Roy, J.-R., Mas-Hesse, J. M. & Walsh, J. R., 2000 A&A 355,891

Leitherer, C. & Heckman, T.M., 1995, ApJS, 96, 9 (LH95)

Lequeux, J., Rayo, J.F., Serrano, A., Peimbert, M. & Torres-Peimbert, S. 1979, A&A, 80, 115

Mac Low, M-M. & Ferrara, A., 1999, ApJ, 513, 142

Maeder, A. 1992, A&A, 264, 105

Marlowe, A. T., Heckman, T. M., Wyse, R. F. G. & Schommer, R., 1995, ApJ, 438, 563

Marlowe, A. T., Meurer G. R., & Heckman, T. M., 1999, ApJ 522, 183

Mas-Hesse, J. M. & Kunth, D., 1999, A&A 349, 765

Moles, M., Aparicio, A. & Mansegosa, J., 1990, A&A 228, 310

Papaderos, P., Loose, H.-H., Thuan, T. X. & Fricke, K. J., 1996, AAS 120, 207

Silich, S. & Tenorio-Tagle, G., 2001, ApJ, 552, 91 (Paper I)

Skillman, E. Kennicutt, R. & Hodge, P., 1989, ApJ 347, 875

Storchi-Bergmann, T., Kinney, A.L., Challis, P., 1995, ApJS 98, 103

Tenorio-Tagle, G., 1996 AJ 111, 1641

Tenorio-Tagle, G., Silich, S., Kunth, D., Terlevich, E. & Terlevich, R., 1999, Mon. Not. Roy. Ast. Soc., 309, 332

Terlevich, R., Terlevich, E. & Denicolo. G., MNRAS (in preparation)

Thuan, T. X. & Martin, G. E., 1981, ApJ 247, 823

van Zee, L., Westpfahl, D., Haynes, M. P. & Salzer, J. J., 1998 AJ 115, 1000

Vilchez, J. M., 1995, AJ 110, 1090

Vilchez, J. M. & Iglesias-Paramo, J., 1998 ApJ 508, 248

This 2-column preprint was prepared with the AAS LaTeX macros v5.0.

Table 1: Star-forming dwarf galaxies. Observational data

Name	M(HI) (10^8 $M_\odot$)	ref	12+Log(O/H)	ref	L(H_α) erg s^{-1}	ref
(1)	(2)	(3)	(4)	(5)	(6)	(7)
Haro-3	5.4	1	8.37	7	7.14×10^{40}	9*
Mkn-49/1318	1.9	1	8.28	14	3.71×10^{40}	10*
NGC-2915	5.9	18	8.4	7	1.30×10^{39}	8
Haro-2	4.6	1	8.4	6	1.20×10^{41}	6*
II-Zw-70	3.4	1	8.07	6	2.23×10^{40}	6*
I-Zw-18	0.26	6	7.18	6	4.29×10^{39}	6*
Haro-14	3.2	1	8.4	13	9.03×10^{39}	9*
IC-10	13	3	8.29	3	2.70×10^{40}	11
GR-8	0.098	4	7.68	15	1.43×10^{38}	9*
DDO-167	0.14	2	7.66	16	7.08×10^{37}	11
DDO-53	0.54	2	7.62	16	6.30×10^{38}	11
WLM	0.56	2	7.74	16	7.40×10^{38}	11
IC-1613	0.49	2	7.86	16	5.25×10^{38}	11
Sex-A	0.79	2	7.49	16	1.40×10^{39}	11
Sex-B	0.44	2	7.56	16	4.07×10^{38}	11
NGC-6822	0.66	2	8.14	16	3.89×10^{39}	11
DDO-47	2.51	2	7.85	16	2.34×10^{38}	11
NGC-2366	7.94	2	7.96	16	1.58×10^{40}	11
NGC-1569	0.59	2	8.16	16	2.19×10^{41}	11
NGC-4214	10.96	2	8.34	16	3.71×10^{40}	11
NGC-4449	13.49	2	8.32	16	7.08×10^{40}	11
NGC-5253	2.04	2	8.27	17	1.97×10^{40}	12*

References: 1) Thuan & Martin, 1981 2) Karachentsev et al., 1999 3) Lequeux et al., 1979 4) Huchtmeier et al., 2000 5) Contini, 1996b 6) Mas-Hesse & Kunth, 1999 7) Papaderos et al., 1996 8) Marlowe et al., 1995 9) Gallagher, Hunter & Bushouse, 1989 10) Vilchez, 1995 11) Hunter, Hawley & Gallagher, 1993 12) Storchi-Bergmann, Kinney & Challis, 1995 13) Marlowe, Meurer & Heckman, 1999 14) Contini, 1996a 15) Moles et al., 1990 16) Skillman, Kennicutt & Hodge, 1989 17) Terlevich, Terlevich & Denicolo, 2001 18) Becker et al., 1988

Table 2: Star-forming dwarf galaxies. Starburst properties

Name	M_{SB} (10^5 $M_\odot$)	L_{mech} (erg s^{-1})	SFR (1-120) ($M_\odot yr^{-1}$)	L_{mech} (erg s^{-1})	Mstar (1-120) (10^5 $M_\odot$)	SFR ($M_\odot yr^{-1}$)	L_{mech} (erg s^{-1})	N_{SB} (exten./coev.)
(1)	(2)	(3)	(4)	(5)	(6)	(7)	(8)	(9)
	Coeval starburst		Extended starburst		Continuous starformation			
Haro-3	5.25	$1.68 \times 10^{+40}$	1.66×10^{-1}	$1.05 \times 10^{+41}$	5546	3.96×10^{-2}	$2.50 \times 10^{+40}$	83/1056
Mkn-49/1318	2.73	$8.74 \times 10^{+39}$	8.64×10^{-2}	$5.45 \times 10^{+40}$	1411	1.01×10^{-2}	$6.36 \times 10^{+39}$	41/517
NGC-2915	9.56×10^{-2}	$3.06 \times 10^{+38}$	3.02×10^{-3}	$1.91 \times 10^{+39}$	6795	4.85×10^{-2}	$3.06 \times 10^{+40}$	5616/71091
Haro-2	8.82	$2.82 \times 10^{+40}$	2.79×10^{-1}	$1.76 \times 10^{+41}$	5298	3.78×10^{-2}	$2.39 \times 10^{+40}$	47/600
II-Zw-70	1.64	$5.24 \times 10^{+39}$	5.19×10^{-2}	$3.27 \times 10^{+40}$	1291	9.22×10^{-3}	$5.82 \times 10^{+39}$	62/788
I-Zw-18	3.15×10^{-1}	$1.01 \times 10^{+39}$	9.97×10^{-3}	$6.29 \times 10^{+39}$	10	7.10×10^{-5}	$4.48 \times 10^{+37}$	2/32
Haro-14	6.64×10^{-1}	$2.12 \times 10^{+39}$	2.10×10^{-2}	$1.33 \times 10^{+40}$	3686	2.63×10^{-2}	$1.66 \times 10^{+40}$	439/5552
IC-10	1.99	$6.35 \times 10^{+39}$	6.28×10^{-2}	$3.96 \times 10^{+40}$	9997	7.14×10^{-2}	$4.51 \times 10^{+40}$	398/5035
GR-8	1.05×10^{-2}	$3.36 \times 10^{+37}$	3.32×10^{-4}	$2.10 \times 10^{+38}$	13	9.14×10^{-5}	$5.76 \times 10^{+37}$	96/1218
DDO-167	5.21×10^{-3}	$1.67 \times 10^{+37}$	1.65×10^{-4}	$1.04 \times 10^{+38}$	17	1.24×10^{-4}	$7.82 \times 10^{+37}$	263/3335
DDO-53	4.63×10^{-2}	$1.48 \times 10^{+38}$	1.47×10^{-3}	$9.25 \times 10^{+38}$	60	4.32×10^{-4}	$2.73 \times 10^{+38}$	103/1306
WLM	5.44×10^{-2}	$1.74 \times 10^{+38}$	1.72×10^{-3}	$1.09 \times 10^{+39}$	85	6.10×10^{-4}	$3.85 \times 10^{+38}$	124/1569
IC-1613	3.86×10^{-2}	$1.24 \times 10^{+38}$	1.22×10^{-3}	$7.71 \times 10^{+38}$	103	7.33×10^{-4}	$4.63 \times 10^{+38}$	210/2660
Sex-A	1.03×10^{-1}	$3.29 \times 10^{+38}$	3.26×10^{-3}	$2.06 \times 10^{+39}$	64	4.57×10^{-4}	$2.88 \times 10^{+38}$	49/621
Sex-B	2.99×10^{-2}	$9.58 \times 10^{+37}$	9.47×10^{-4}	$5.98 \times 10^{+38}$	42	3.03×10^{-4}	$1.91 \times 10^{+38}$	112/1416
NGC-6822	2.86×10^{-1}	$9.15 \times 10^{+38}$	9.05×10^{-3}	$5.71 \times 10^{+39}$	310	2.22×10^{-3}	$1.40 \times 10^{+39}$	86/1084
DDO-47	1.72×10^{-2}	$5.51 \times 10^{+37}$	5.44×10^{-4}	$3.44 \times 10^{+38}$	512	3.66×10^{-3}	$2.31 \times 10^{+39}$	2351/29755
NGC-2366	1.16	$3.72 \times 10^{+39}$	3.68×10^{-2}	$2.32 \times 10^{+40}$	2193	1.57×10^{-2}	$9.88 \times 10^{+39}$	149/1887
NGC-1569	$1.61 \times 10^{+1}$	$5.15 \times 10^{+40}$	5.10×10^{-1}	$3.22 \times 10^{+41}$	295	2.11×10^{-3}	$1.33 \times 10^{+39}$	1/18
NGC-4214	2.73	$8.74 \times 10^{+39}$	8.64×10^{-2}	$5.45 \times 10^{+40}$	10073	7.19×10^{-2}	$4.54 \times 10^{+40}$	291/3688
NGC-4449	5.21	$1.67 \times 10^{+40}$	1.65×10^{-1}	$1.04 \times 10^{+41}$	11533	8.24×10^{-2}	$5.20 \times 10^{+40}$	175/2215
NGC-5253	1.45	$4.64 \times 10^{+39}$	4.59×10^{-2}	$2.89 \times 10^{+40}$	1464	1.05×10^{-2}	$6.60 \times 10^{+39}$	80/1010

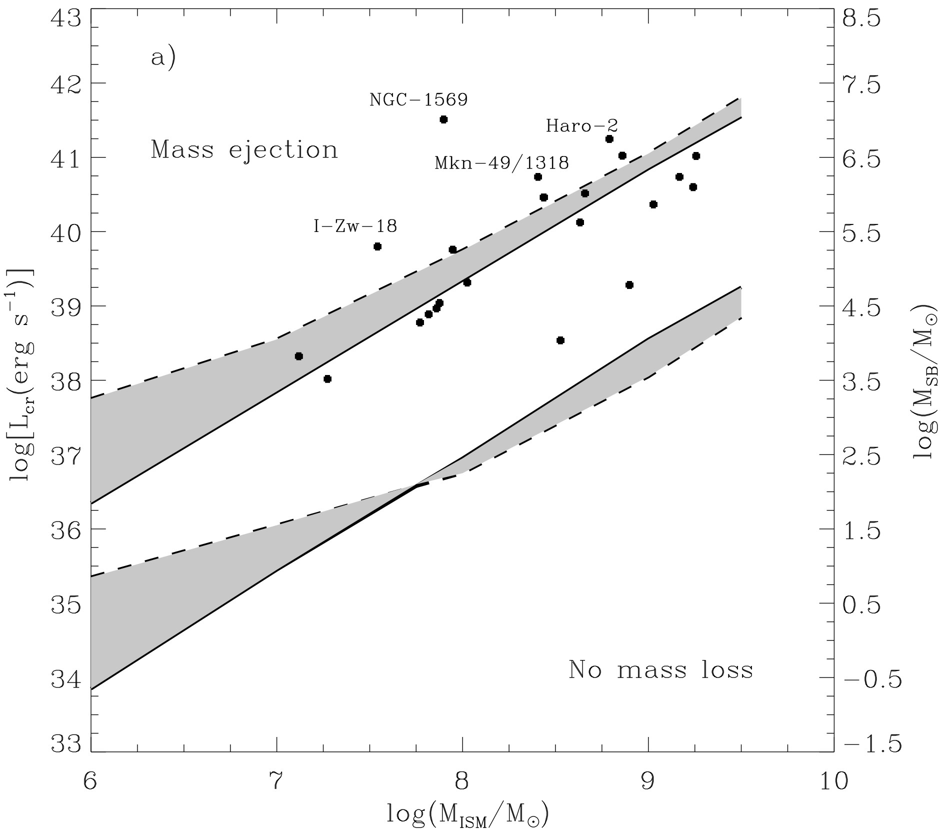
a)
Mass ejection
No mass loss
NGC-1569
Haro-2
Mkn-49/1318
I-Zw-18
$\log[L_{cr}(\mathrm{erg\ s^{-1}})]$
$\log(M_{SB}/M_\odot)$
$\log(M_{ISM}/M_\odot)$
43
42
41
40
39
38
37
36
35
34
33
8.5
7.5
6.5
5.5
4.5
3.5
2.5
1.5
0.5
−0.5
−1.5
6
7
8
9
10

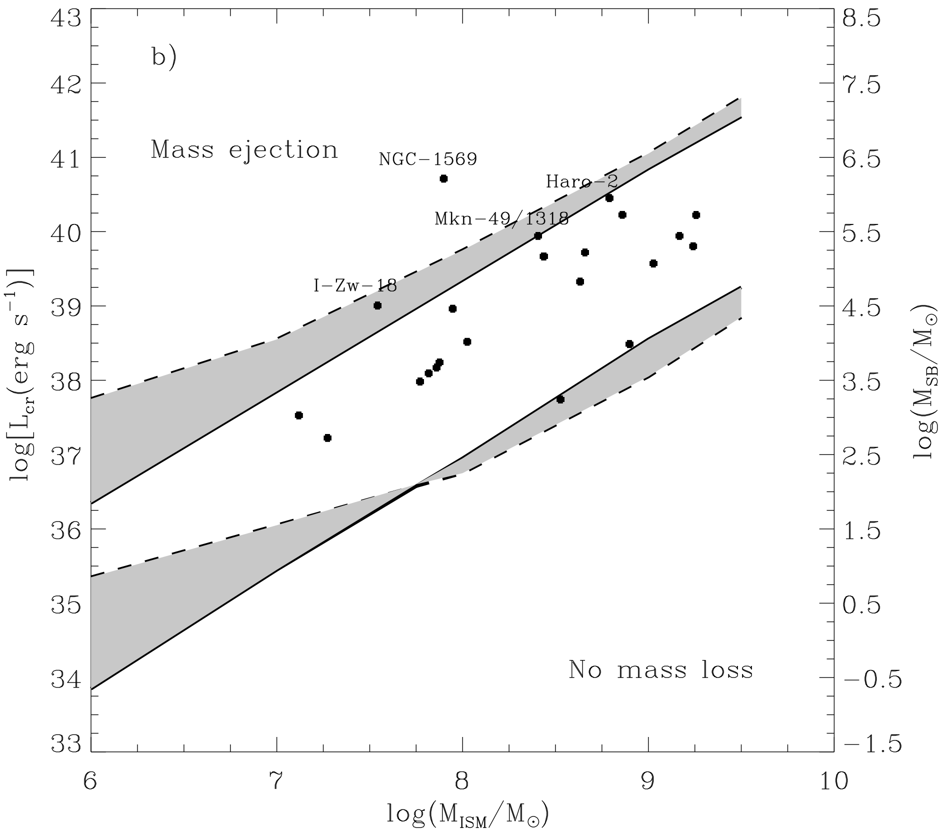
b)
Mass ejection
No mass loss
NGC-1569
Haro-2
Mkn-49/I318
I-Zw-18
$\log[L_{cr}(\mathrm{erg\ s^{-1}})]$
$\log(M_{SB}/M_\odot)$
$\log(M_{ISM}/M_\odot)$
33
34
35
36
37
38
39
40
41
42
43
−1.5
−0.5
0.5
1.5
2.5
3.5
4.5
5.5
6.5
7.5
8.5
6
7
8
9
10

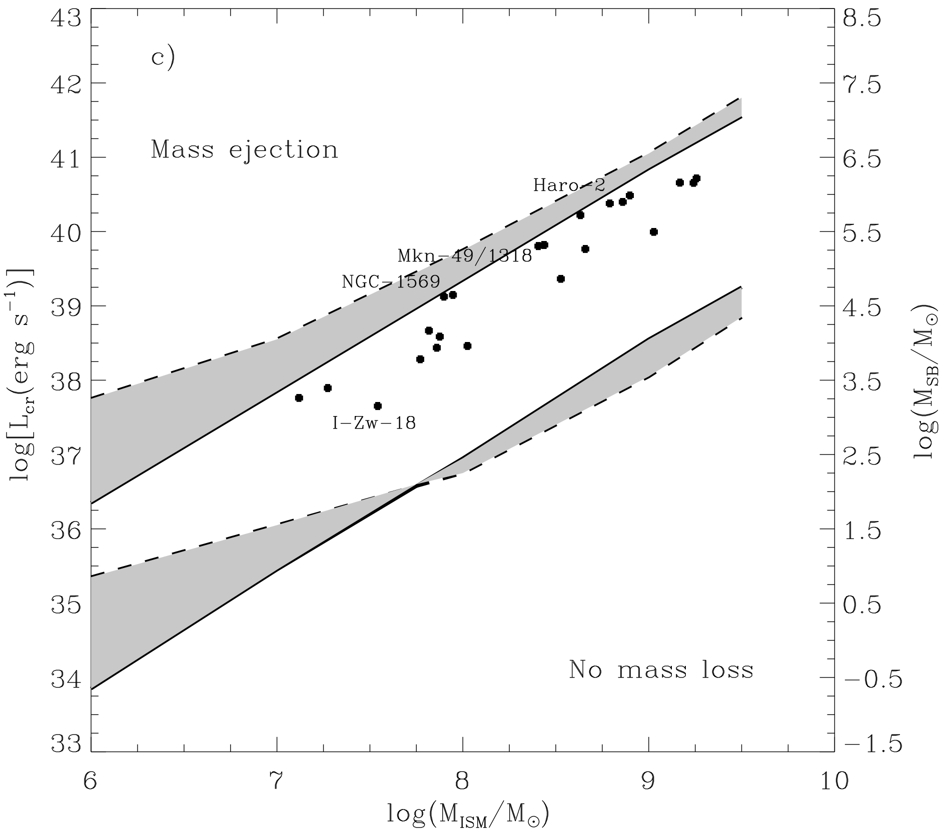

Fig. 1.— Energy estimates. The log of the critical mechanical luminosity (left-hand side axis) and mass of the star cluster M_{SB} (right-hand side axis), required to eject matter from galaxies with a M_{ISM} in the range 10^6 – 10^{10} $M_\odot$. The lower limit estimates are shown for galaxies with extreme ISM density distributions: flattened disks (lower two lines), and spherical galaxies without rotation (upper lines), for two values of the intergalactic pressure $P_{IGM}/k = 1$ cm^{-3} K (solid lines) and $P_{IGM}/k = 100$ cm^{-3} K (dashed lines). Each line should be considered separately (see Paper I) as they divide the parameter space into two distinct regions: a region of no mass loss that is found below the line and a region in which blowout and mass ejection occur is found above each line. a) – c) Estimates for models 1 – 3, respectively.